In Planta Analysis of the Cell Cycle-Dependent Localization of AtCDC48A and Its Critical Roles in Cell Division, Expansion, and Differentiation[1][W][OA]

Sookhee Park, David Michael Rancour*, and Sebastian York Bednarek

Department of Biochemistry (S.P., D.M.R., S.Y.B.) and Program in Cellular and Molecular Biology (S.P., S.Y.B.), University of Wisconsin, Madison, Wisconsin 53706

CDC48/p97 is a conserved homohexameric AAA-ATPase chaperone required for a variety of cellular processes but whose role in the development of a multicellular model system has not been examined. Here, we have used reverse genetics, visualization of a functional Arabidopsis (*Arabidopsis thaliana*) CDC48 fluorescent fusion protein, and morphological analysis to examine the subcellular distribution and requirements for AtCDC48A in planta. Homozygous *Atcdc48A* T-DNA insertion mutants arrest during seedling development, exhibiting decreased cell expansion and displaying pleiotropic defects in pollen and embryo development. *Atcdc48A* insertion alleles show significantly reduced male transmission efficiency due to defects in pollen tube growth. Yellow fluorescent protein-AtCDC48A, a fusion protein that functionally complements the insertion mutant defects, localizes in the nucleus and cytoplasm and is recruited to the division mid-zone during cytokinesis. The pattern of nuclear localization differs according to the stage of the cell cycle and differentiation state. Inducible expression of an *Atcdc48A* Walker A ATPase mutant in planta results in cytokinesis abnormalities, aberrant cell divisions, and root trichoblast differentiation defects apparent in excessive root hair emergence. At the biochemical level, our data suggest that the endogenous steady-state protein level of AtCDC48A is dependent upon the presence of ATPase-active AtCDC48A. These results demonstrate that CDC48A/p97 is critical for cytokinesis, cell expansion, and differentiation in plants.

Members of the AAA (ATPase associated with different cellular activities)-ATPase protein family are characterized by either one (type I) or two (type II) 220 to 250 amino acid ATPase domains containing both conserved Walker A and B motifs per protomer (Beyer, 1997; Neuwald et al., 1999). The ATPase domains elicit protein conformational changes upon the nucleotide binding, hydrolysis, and product release that is believed to be required for the function of the mechanochemical enzyme (Rouiller et al., 2000, 2002; Zhang et al., 2000; Beuron et al., 2003, 2006; DeLaBarre and Brunger, 2003, 2005; Huyton et al., 2003; Wang et al., 2003; Davies et al., 2005). The conservation and widespread use of the AAA domain suggests that AAA-ATPase proteins may use common mechanisms that utilize their ATPase activity to carry out a wide range of cellular functions (Lupas and Martin, 2002).

CDC48/p97 is a highly abundant type II AAA-ATPase (Peters et al., 1990) involved in cell cycle control (Moir et al., 1982) and cell proliferation (Egerton and Samelson, 1994). Gene disruption of *CDC48/p97* in budding and fission yeasts (*Saccharomyces cerevisiae* and *Schizosaccharomyces pombe*; Fröhlich et al., 1991; Ikai and Yanagida, 2006), trypanosomes (TbVCP; Lamb et al., 2001), mouse (Muller et al., 2007), and *Drosophila* (*ter94*; Leon and McKearin, 1999) demonstrates that CDC48/p97 is essential in unicellular and multicellullar organisms. At the molecular level, CDC48/p97 is involved in many distinct cellular processes (Woodman, 2003; Dreveny et al., 2004; Meyer, 2005; Jentsch and Rumpf, 2007). Current models indicate that the targeting of CDC48/p97 family members to cellular pathways is accomplished via recruitment by adapter proteins or cofactors. For example, in mammalian cells, CDC48/p97 requires the cofactor p47 to mediate endoplasmic reticulum (ER) and Golgi membrane assembly (Kondo et al., 1997; Roy et al., 2000; Yuan et al., 2001) and nuclear envelope reformation (Hetzer et al., 2001). An additional cofactor complex, Ufd1-Npl4, is required for p97-mediated formation of the chromatin-associated nuclear envelope network, consolidation of the nuclear envelope (Hetzer et al., 2001), mitotic spindle dynamics (Cao et al., 2003; Cao and Zheng, 2004; Cheeseman and Desai, 2004), and ER-associated protein degradation (Alzayady et al., 2005; Schuberth and Buchberger, 2005; Römisch, 2006).

Mutations in CDC48/p97-interacting proteins have provided insight into the physiological and develop-

[1] This work was supported by the National Science Foundation (grant nos. 0542034 [for Arabidopsis Biological Resource Center material distribution] and DBI–0421266), and by the Department of Energy, Division of Energy Biosciences (grant no. DE–FG02–ER20332 to S.Y.B.).

* Corresponding author; e-mail drancour@wisc.edu.

The author responsible for distribution of materials integral to the findings presented in this article in accordance with the policy described in the Instructions for Authors (www.plantphysiol.org) is: Sebastian York Bednarek (sybednar@wisc.edu).

[W] The online version of this article contains Web-only data.

[OA] Open Access articles can be viewed online without a subscription.

www.plantphysiol.org/cgi/doi/10.1104/pp.108.121897

mental functions of CDC48/p97-dependent biochemical pathways. *eyes closed*, a loss-of-function allele of the *Drosophila* p47 adapter protein ortholog (Sang and Ready, 2002), shows nuclear envelope assembly defects in early zygotic divisions in *Drosophila*. In Arabidopsis (*Arabidopsis thaliana*), loss of PUX1, a negative regulator of CDC48/p97 function (Rancour et al., 2004; Park et al., 2007), results in accelerated plant growth due to increased cell division and expansion (Rancour et al., 2004).

Plant morphological development requires the coordination of cell division, expansion, and differentiation (Meijer and Murray, 2001; Beemster et al., 2003; Fleming, 2006). Our previous work has suggested that AtCDC48 may be directly involved in cell division and expansion (Rancour et al., 2002, 2004). The Arabidopsis genome encodes three *CDC48* isoforms: *AtCDC48A* (At3g09840), *AtCDC48B* (At3g53230), and *AtCDC48C* (At5g03340). These isoforms are predicted to share 91% (AtCDC48B) and 95% (AtCDC48C) amino acid identity to AtCDC48A (Rancour et al., 2002). Expression of *AtCDC48A* mRNA is highest in proliferating cells of the vegetative shoot, root, and flowers in rapidly growing plants (Feiler et al., 1995; Zimmermann et al., 2004, 2005).

At the subcellular level, AtCDC48A has been shown by immunofluorescence microscopy to be localized to the cytoplasm, nucleus, and to the phragmoplast midzone during cytokinesis (Feiler et al., 1995; Rancour et al., 2002). In addition, overexpression studies in plant protoplasts of fluorescent fusion protein-tagged AtCDC48A have suggested that the chaperone is associated with the ER and plasma membrane (Aker et al., 2006, 2007).

The role of the CDC48/p97 protein family during growth and development has not been examined to date in planta. Here, we show, through live-cell imaging and the expression and analysis of loss-of-function and inducible dominant-negative ATPase-defective mutants, that AtCDC48A is essential for plant growth and development at various stages.

These results provide evidence for CDC48/p97 function in plant cytokinesis, cell expansion, and differentiation. In addition, our data support a role for AtCDC48A ATPase function in maintenance of steady-state AtCDC48A protein levels, thus suggesting a mode of protein turnover autoregulation.

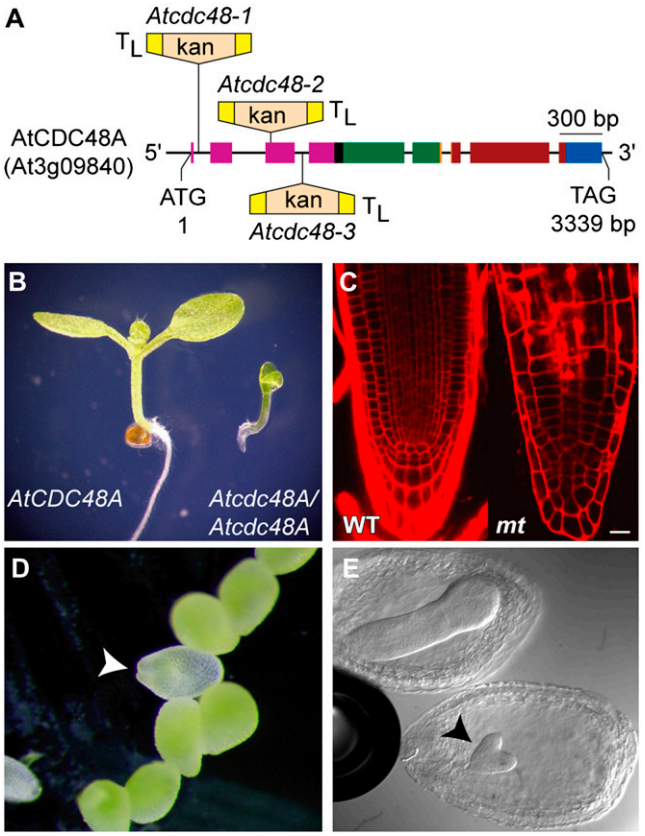

Figure 1. Schematic representation of *Atcdc48A*$^{T\text{-}DNA}$ mutant alleles and the phenotypes of *Atcdc48A*$^{T\text{-}DNA}$ seedlings, seeds, and embryos. A, The exon/intron gene structure of *AtCDC48A* is shown to scale with broad-colored boxes representing exons and black inter-exon thin lines representing introns. The colors of the exons correspond to the DNA-coding regions encoding the protein domains of AtCDC48A: pink, N terminus; black, linker 1; green, D1 ATPase; orange, linker 2; red, D2 ATPase; blue, C terminus. The position and directions of T-DNA inserts with left border sequences are indicated (T_L). T-DNAs are not drawn to scale. kan, T-DNA neomycin phosphotransferase selectable gene marker. B, Stereo micrograph of 5-d-old wild-type *AtCDC48A* and homozygous *Atcdc48A*$^{T\text{-}DNA}$ mutant seedlings. Homozygous *Atcdc48A*$^{T\text{-}DNA}$ plants die soon after this stage of development. C, Roots of 5-d-old wild-type *AtCDC48A* (WT) and homozygous *Atcdc48A*$^{T\text{-}DNA}$ mutant (*mt*) plants stained with propidium iodide and imaged by LSCM. The mutant root image comprises the entire root length (as shown in B), while the left image corresponds to only tip of the wild type. Scale bar = 10 μm. D, Stereo micrograph of a portion of an immature silique from a self-fertilized heterozygous *Atcdc48A*$^{T\text{-}DNA}$ plant approximately 10 d after fertilization. A pale green *Atcdc48A* homozygous seed is indicated by an arrowhead. E, Sibling embryos of an immature silique (approximately 5 d after fertilization) from a self-fertilized heterozygous *Atcdc48A*$^{T\text{-}DNA}$ plant. Mutant embryo development is shown arrested at the heart stage (arrowhead).

RESULTS

Molecular Characterization and Phenotypic Analysis of *Atcdc48A* T-DNA Insertion Mutants

The gene encoding *AtCDC48A* is 3.3 kb in length and composed of eight exons (Fig. 1A). To characterize the biological function of AtCDC48A, we identified three independent *Atcdc48A* T-DNA insertion lines (*Atcdc48A*$^{T\text{-}DNA}$*-1*, *Atcdc48A*$^{T\text{-}DNA}$*-2*, and *Atcdc48A*$^{T\text{-}DNA}$*-3*). All three *Atcdc48A* alleles exhibited identical phenotypes. The T-DNA insertion site in each of the alleles was verified by PCR amplification and DNA sequence analysis. The T-DNAs in *Atcdc48A*$^{T\text{-}DNA}$*-1*, *Atcdc48A*$^{T\text{-}DNA}$*-2*, and *Atcdc48A*$^{T\text{-}DNA}$*-3* were inserted in the first intron, third exon, and third intron, respectively, of *AtCDC48A* (Fig. 1A). All three T-DNA insertion sites are upstream of the sequences encoding the

two ATPase domains. No viable soil-grown homozygous plants for any of the *Atcdc48A*$^{T\text{-}DNA}$ insertion alleles were identified from progeny of self-fertilized heterozygous parent plants. To verify that the mutant alleles are recessive, progeny from self-fertilized heterozygous *Atcdc48A*$^{T\text{-}DNA}$ mutants were grown on solid Murashige and Skoog media (Murashige and Skoog, 1962) and were monitored for growth. Approximately 4% of the germinated seedlings (14 seedlings from 346 seeds plated) on solid Murashige and Skoog media were homozygous for the T-DNA insertion. Homozygous *Atcdc48A*$^{T\text{-}DNA}$ seedlings arrested 1 d after germination, and the mutants exhibited severely disorganized root morphology (Fig. 1B). As shown in Figure 1B, roots of homozygous *Atcdc48A*$^{T\text{-}DNA}$ mutants were less than 0.5 mm in length with a root tip that was narrower than wild-type (Fig. 1C). Morphologically, *Atcdc48A*$^{T\text{-}DNA}$ mutant roots displayed abnormal cell files, with no apparent elongation or meristematic regions and a disorganized root cap (Fig. 1C). These results indicated that AtCDC48A is critical for seedling development and growth.

The allelic ratio of F_1 progeny from a self-fertilized heterozygous *Atcdc48A*$^{T\text{-}DNA}$/+ plant did not follow the predicted frequency of segregation for a typical recessive mutation, suggesting earlier defects in development. Therefore, 10 d after flowering, immature siliques from two generations of self-fertilized heterozygous plants (approximately 40 siliques of each generation) were examined. In a visual survey of seeds from heterozygous *Atcdc48A*$^{T\text{-}DNA}$ siliques, pale-green seeds, suggesting embryo development defects (Meinke, 1994; http://www.seedgenes.org/Tutorial.html), were observed at a frequency of five pale seeds out of 60 total (approximately 8%; Fig. 1D). PCR-based genotypic analysis of embryos from the pale-green seeds indicated they were homozygous for the *Atcdc48A*$^{T\text{-}DNA}$ insertions (Supplemental Fig. S1). To determine at which stage in embryo development homozygous *Atcdc48A*$^{T\text{-}DNA}$ mutants arrested, 5-d-postfertilization siliques from wild-type and heterozygous *Atcdc48A*$^{T\text{-}DNA}$/+ mutant plants were cleared with Hoyers solution (Liu and Meinke, 1998) and examined by light microscopy using differential interference contrast (DIC) optics. *Atcdc48A*$^{T\text{-}DNA}$ mutant embryo growth was arrested at the early heart stage of development (Fig. 1E), supporting a role for AtCDC48A in plant embryogenesis.

PCR-based genotype analysis of 10-d-old soil-grown surviving progeny from self-fertilized heterozygous *Atcdc48A*$^{T\text{-}DNA}$/+ plants showed an altered segregation ratio (78 wild type:114 heterozygote [41%:59%, respectively]; $n = 192$) in contrast to the predicted frequency for a recessive embryo/seedling lethal mutation (1 wild type:2 heterozygote [33%:67%, respectively]). The altered segregation ratio suggests impairment of mutant allele transmission through the gametes. To confirm this, male and female transmission efficiencies of the *Atcdc48A*$^{T\text{-}DNA}$ alleles were determined by performing reciprocal crosses between heterozygous mutants and wild-type plants. Pollen grains from the wild-type plants were able to fertilize *Atcdc48A*$^{T\text{-}DNA}$/+ plants to yield progeny that segregated in the ratio of 1:0.73 (124 wild type:91 heterozygote [58%:42%, respectively]; $n = 215$). Using *Atcdc48A*$^{T\text{-}DNA}$/+ pollen to fertilize wild-type stigmas resulted in a highly skewed segregation of progeny genotype (235 wild-type:13 heterozygote [95%:5%, respectively]; $n = 248$). *Atcdc48A*$^{T\text{-}DNA}$ alleles show significantly reduced male transmission efficiency and modest female transmission efficiency defects. These results suggest a critical role for AtCDC48A in pollen development and/or function.

Analysis of Pollen Development in *Atcdc48A* Mutants

To determine at which developmental stage *Atcdc48A*$^{T\text{-}DNA}$ pollen was defective, the development, maturation, and germination of pollen grains from wild-type and heterozygous *Atcdc48A*$^{T\text{-}DNA}$/+ plants were analyzed by DIC and epifluorescence microscopy. Staining of nuclear DNA with 4,6-diamidino-2-phenylindole (DAPI) was used to analyze pollen developmental progression. No apparent defects in late microsporogenesis, including tetrad formation and microspore release, were observed compared to wild type. After microspore release and pollen mitosis I and II, all the pollen grains from wild-type and *Atcdc48A*$^{T\text{-}DNA}$/+ plants contained two generative and one vegetative nucleus (Fig. 2A) and thus appeared normal. To investigate whether *Atcdc48A*$^{T\text{-}DNA}$ mutant pollen arrest at an early developmental stage prior to late microsporogenesis (meiosis II) or, alternatively, during stages after pollen mitosis II, the *Atcdc48A*$^{T\text{-}DNA}$*-1* and *quartet* (*qrt*) mutant alleles were introgressed by cross-pollination between heterozygous *Atcdc48A*$^{T\text{-}DNA}$*-1*/+ and *qrt* mutant plants. The *qrt* mutation results in pollen grains that remain physically associated in a tetrad and undergo synchronous development due to a defect in the pollen mother cell wall that results in microspore dissociation failure after meiosis II (Preuss et al., 1994; Rhee and Somerville, 1998). Pollen from wild-type *qrt* (*AtCDC48A;qrt*) and heterozygous *Atcdc48A*$^{T\text{-}DNA}$*-1*/+*;qrt* lines was monitored by bright-field microscopy (Fig. 2, B and C). As shown, four pollen grains of *Atcdc48A*$^{T\text{-}DNA}$*-1*/+*;qrt* remained associated, indicating that the *Atcdc48A*$^{T\text{-}DNA}$*-1* mutation does not disrupt meiotic processes in pollen development.

To test whether pollen germination was affected by the *Atcdc48A*$^{T\text{-}DNA}$*-1* insertion mutation, in vitro pollen germination assays were performed. Pollen tubes were observed protruding from all four germinating wild-type *AtCDC48A;qrt* pollen grains (Fig. 2B). In contrast, only two pollen grains germinated from *Atcdc48A*$^{T\text{-}DNA}$*-1*/+*;qrt* pollen (Fig. 2C), with approximately 5% showing delayed growth of a third pollen tube (Fig. 2C, arrows). These data indicate a critical role for AtCDC48A in pollen germination and tube elongation that manifests in significant transmission inhibition of the *Atcdc48A*$^{T\text{-}DNA}$ insertion alleles.

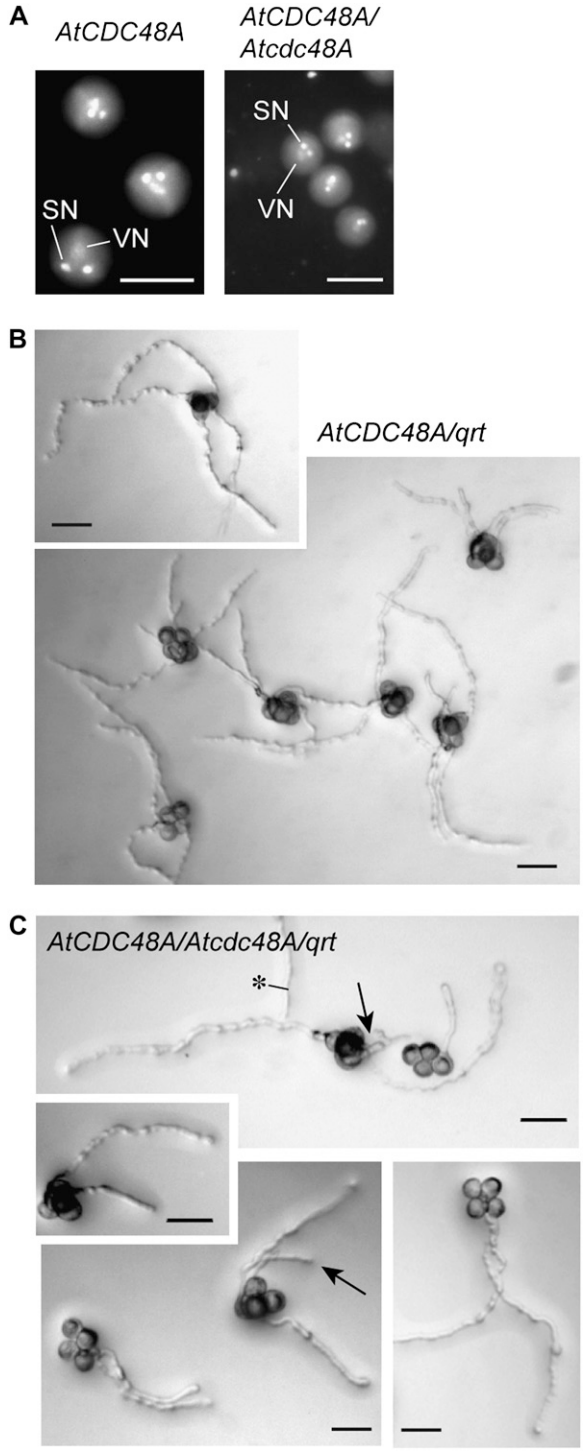

Figure 2. Analysis of development and tube germination of pollen from *AtCDC48A* and heterozygous *Atcdc48A* plants. A, Pollen grains from wild-type (left) and heterozygous *Atcdc48A*$^{T\text{-}DNA}$ (right) plants were examined at onset of desiccation by epifluorescence microscopy after DAPI staining. SN, Sperm nuclei; VN, vegetative nucleus. Scale bars = 15 μm. B and C, Pollen grains from *qrt* (*AtCDC48A;qrt*; B) and heterozygous *Atcdc48A*$^{T\text{-}DNA}$*;qrt* (*Atcdc48A/+;qrt*; C) plants were germinated on pollen germination media at 28°C for 24 h and then imaged with DIC optics. Arrows indicate *Atcdc48A* mutant pollen tubes. Asterisk indicates a pollen tube from outside the field of view. Scale bars = 50 μm.

Characterization and Localization of Native Promoter::YFP-AtCDC48A in Homozygous *Atcdc48A*$^{T\text{-}DNA}$ Seedlings

To examine the tissue and subcellular localization of AtCDC48A, transgenic Arabidopsis plants expressing an N-terminal tagged yellow fluorescent protein (YFP; Heim and Tsien, 1996) AtCDC48A fusion protein (YFP-AtCDC48A) under control of the native *AtCDC48A* promoter were generated. This construct was introduced into heterozygous *Atcdc48A*$^{T\text{-}DNA}$/+ plants, and the T_2 population was analyzed by both YFP screening and PCR genotyping (Supplemental Fig. S2) to assess complementation. The YFP-AtCDC48A construct rescued all the phenotypic defects associated with the *Atcdc48A*$^{T\text{-}DNA}$ mutants described above. Immunoblot analysis of protein extracts prepared from wild-type and *Atcdc48A;YFP-AtCDC48A* seedlings using anti-AtCDC48A and -GFP antibodies confirmed that the 118-kD YFP-AtCDC48A fusion protein was intact (Supplemental Fig. S3).

Expression of YFP-AtCDC48A was detected throughout developing *Atcdc48A*$^{T\text{-}DNA}$*/Atcdc48A*$^{T\text{-}DNA}$*;YFP-AtCDC48A* transgenic plants (Fig. 3; Supplemental Movies S1–S4) and is consistent with publicly available gene expression data (Supplemental Fig. S4). YFP-AtCDC48A fusion protein localizes to the nucleus and cytoplasm of all cells throughout all tissues of the seedling, including leaves, the shoot apical meristem (Fig. 3A; Supplemental Movie S1), and the root (Fig. 3, B–D; Supplemental Movies S3 and S4). In addition, YFP-AtCDC48A fusion protein was observed in developing ovules, pollen sacs, and pollen in mature plants. In germinating pollen, YFP-AtCDC48A was detected in the vegetative nucleus and surrounding the nuclear periphery but was not detected in the two sperm nuclei. Additionally, YFP-AtCDC48A was localized to the growing tip of the pollen tubes (Fig. 3E; Supplemental Movie S2).

Upon closer examination in root cells, YFP-AtCDC48A subcellular localization was cell cycle dependent. During mitosis, YFP-AtCDC48A was associated with the mitotic spindle (Fig. 3C, arrow) and subsequently with the phragmoplast mid-zone during cytokinesis (Fig. 3, C and D, arrowhead). During karyokinesis, YFP-AtCDC48A containing vesicle-like structures began to localize and coalesce around the chromosomal material (Fig. 3, D and F; Supplemental Movie S3). Following cell division, YFP-AtCDC48A was associated with the nuclear envelope, nucleoplasm, and nucleolar cavity (Fig. 3, C, D, F, and G; Supplemental Movie S3).

Phenotypic Analysis of Transgenic *Atcdc48A* Dominant-Negative Mutant Plants

Loss-of-function insertion alleles of *Atcdc48*$^{T\text{-}DNA}$*-1*, *Atcdc48*$^{T\text{-}DNA}$*-2*, and *Atcdc48*$^{T\text{-}DNA}$*-3* display early pleiotropic developmental phenotypes. To examine the role of AtCDC48A in later stages of plant development,

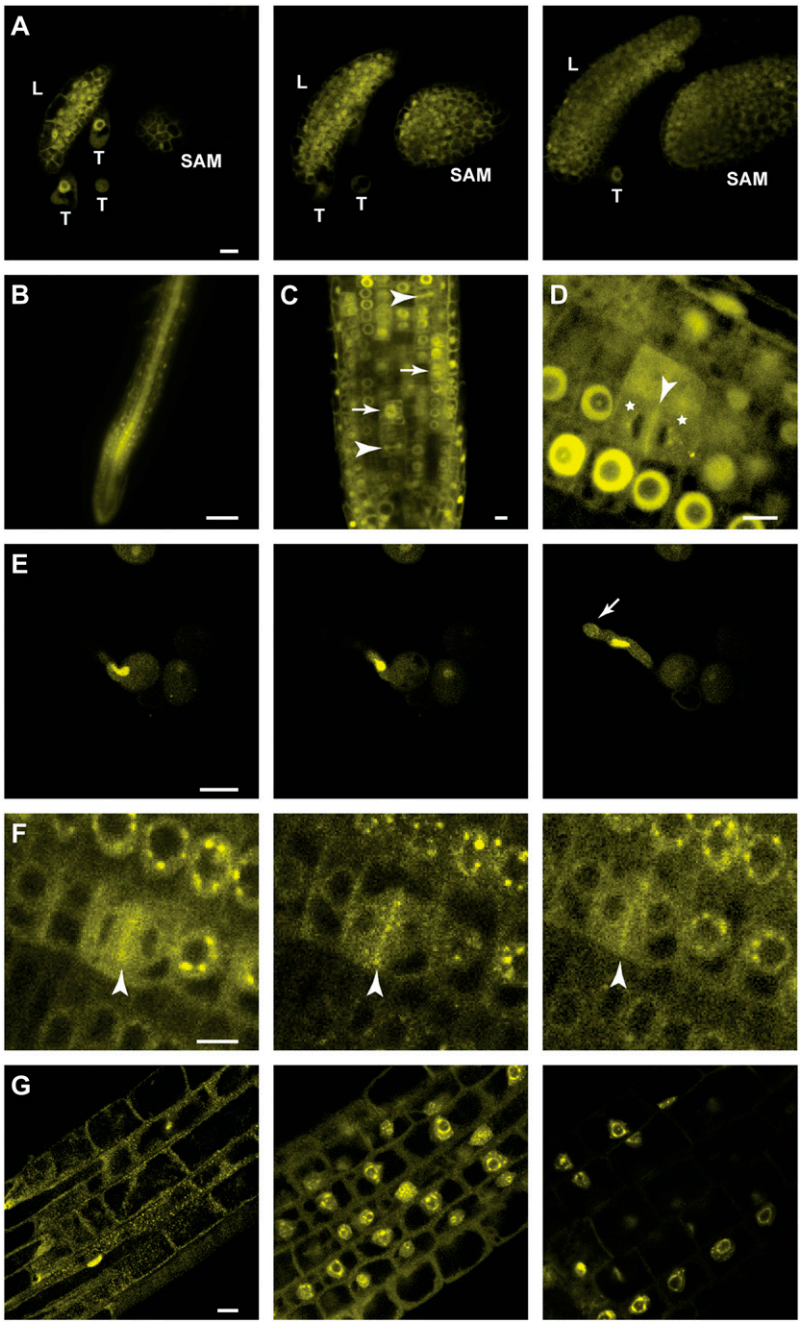

Figure 3. Localization of YFP-AtCDC48A in transgenic homozygous *Atcdc48A*$^{T\text{-}DNA}$ seedlings. Transgenic T_3 seedlings were examined 3 d after germination. A, Representative LSCM images of YFP-AtCDC48A expressed in leaves (L), trichomes (T), and the shoot apical meristem (SAM). Scale bar = 10 μm. The three segments correspond to the first (left), middle, and last (right) images of a serial Z-stack set taken down the vertical axis of the plant. See Supplemental Movie S1 for complete Z-stack series of images. B, Expression of YFP-AtCDC48A in the root visualized by wide-field fluorescence microscopy. Scale bar = 100 μm. C and D, YFP-AtCDC48A expression in the root division zone visualized by LSCM. Scale bar = 10 μm. Division plane localization is indicated by arrowheads. Spindle localization is indicted by arrows. Asterisks indicate vesicle-like structures located neighboring developing nuclear membranes. E, The vegetative nucleus during pollen tube elongation. The three segments correspond to the first (left), middle, and last (right) images of a time series taken during pollen tube elongation in vitro. See Supplemental Movie S2 for complete time series. Arrow indicates the tip of the pollen tube. Scale bar = 10 μm. F, YFP-AtCDC48A localization during karyokinesis in dividing root cells. The three segments correspond to the first (left), middle, and last (right) images of a time series taken during root cell division. See Supplemental Movie S3 for complete time series. Arrowhead indicates a dividing cell division plane. Scale bar = 10 μm. G, YFP-AtCDC48A nucleus localization in the primary root elongation zone. The three segments correspond to the first (left), middle, and last (right) images of a serial Z-stack set taken perpendicular to the root radial axis. See Supplemental Movie S4 for complete Z-stacks. Scale bar = 10 μm.

transgenic plants expressing dominant-negative mutant Atcdc48A proteins (Atcdc48A^{DN}) under the control of an ethanol-inducible promoter system from *Aspergillus nidulans* (Caddick et al., 1998; Roslan et al., 2001) were generated. Using this system, the function of endogenous AtCDC48A was temporally inactivated during the seedling and later stages of plant development, thus circumventing the gametophyte and seedling lethal phenotypes encountered with the *Atcdc48A*$^{T\text{-}DNA}$ loss-of-function insertion alleles. Previous studies have demonstrated that the incorporation of cdc48/p97 D1 and D2 ATP binding and hydrolysis mutant subunits into endogenous CDC48/p97 hexameric complexes disrupts their function in vivo and in vitro (Lamb et al., 2001; Dalal et al., 2004; Park et al., 2007), and thus function as dominant-negative proteins (subunits). Ethanol-inducible AtCDC48A (H6T7-WT), Atcdc48A$^{DN\text{-}H}$ (H6T7-DN-H; ATP hydrolysis [E308Q/E581Q]), and Atcdc48A$^{DN\text{-}B}$ (H6T7-DN-B; ATP binding [K254A/K572A]) plant expression constructs contained an N-terminal six His and T7 (H6T7) tandem epitope tag to facilitate immunological detection of the transgene products. In the absence of ethanol, H6T7-tagged wild-type and Atcdc48A$^{DN\text{-}H,\ -B}$ mutant proteins were not detected by immunoblot analysis (Fig. 4A, lanes 1, 4, and 7). Upon the addition

of (2%) ethanol to the growth medium, expression of H6T7-tagged wild-type AtCDC48A and Atcdc48A$^{DN-H, -B}$ proteins were readily detected after 6 h (Fig. 4A, lanes 2, 5, and 8), and after approximately 24 h the levels of H6T7-DN mutant protein (Fig. 4A, lanes 3, 6, and 9) were approximately 10-fold higher than H6T7-WT based on densitometric immunoblot analysis. Induction of H6T7-tagged wild-type and Atcdc48A$^{DN-H, -B}$ mutant proteins did not vary over an ethanol application range of 0.5% to 2% (v/v). In addition, untransformed seedling growth was not affected under any of the induction conditions used.

After 48 h of post-ethanol treatment, steady-state levels of total AtCDC48A protein (Fig. 4B, top) are highly elevated in lines expressing H6T7-DN protein (Fig. 4B, lanes 4–7). Parallel ethanol treatment of H6T7-WT protein-expressing lines (Fig. 4B, lanes 2 and 3) shows that total AtCDC48A protein levels are similar to wild-type plants (Fig. 4B, lane 1). In lines expressing H6T7-DN proteins, the levels of endogenous AtCDC48 and transgene H6T7-AtCDC48-DN protein products was greatly increased relative to H6T7-WT (Fig. 4B, middle anti-T7, compare lanes 2 and 3–7). DRP1A protein detection was used as a loading control (Fig. 4B, bottom).

To determine if the elevated levels of H6T7-DN proteins, relative to H6T7-WT, were due to altered transcript levels for the transgenes, reverse transcription-PCR analysis was performed on total RNA from ethanol-treated transgenic seedlings (Fig. 4C). Expression of transgenic *Atcdc48* mRNA was detected 2 h after ethanol induction (Fig. 4C, lanes 2, 6, and 10) and increased steadily over the 24-h time course (Fig. 4C, lanes 3 and 4, 7 and 8, and 11 and 12). mRNA expression levels were comparable between wild-type and mutant transgenes.

Transgenic plants expressing wild-type AtCDC48A (H6T7-WT) exhibited no abnormal phenotypes (Fig. 5, B, D and F; Supplemental Fig. S5). In contrast, transgenic plants expressing either Atcdc48A^{DN-B} or Atcdc48A^{DN-H} exhibited aberrant morphological phenotypes in both the aerial and root regions of the plant (Fig. 5, A, C, E, and G; Supplemental Fig. S5). As shown in Figure 5A, the cotyledons of seedlings expressing *H6T7-DN-B* stopped expanding and became chlorotic as compared to plants expressing *H6T7-WT*, the wild-type control (Fig. 5B; Supplemental Fig. S5). *H6T7-DN-B* trichomes were primarily bibranched and smaller when compared to those from AtCDC48A plants (Fig. 5, C and D, respectively). Roots of *H6T7-DN-B* plants displayed altered root hair morphology, frequency, and distribution (Fig. 5, E, compared to wild-type right segment, F). Seedling roots expressing *H6T7-DN-B* protein showed an enhanced number of epidermal cell root hairs (Fig. 5, E and G) relative to root expressing *H6T7-WT* (Fig. 5F). In addition, root growth arrested upon induction of *H6T7-DN-B* and *H6T7-DN-H* dominant-negative protein expression relative to H6T7-WT (Fig. 5H). *H6T7-DN-H* plants exhibited less severe phenotypes overall than *H6T7-DN-B* plants, including root length (Fig. 5H), excessive root hair emergence, and aerial yellowing as observed in the *H6T7-DN-B* plants (Supplemental Fig. S5).

Analysis of the Effects of *Atcdc48^{DN-B}* Expression on Root Cell Development

To further investigate the morphology of seedlings expressing Atcdc48A^{DN-B}, root cross sections from plants before and after ethanol induction were examined via microscopic analysis. Transverse sections of seedling roots from plants expressing H6T7-WT and

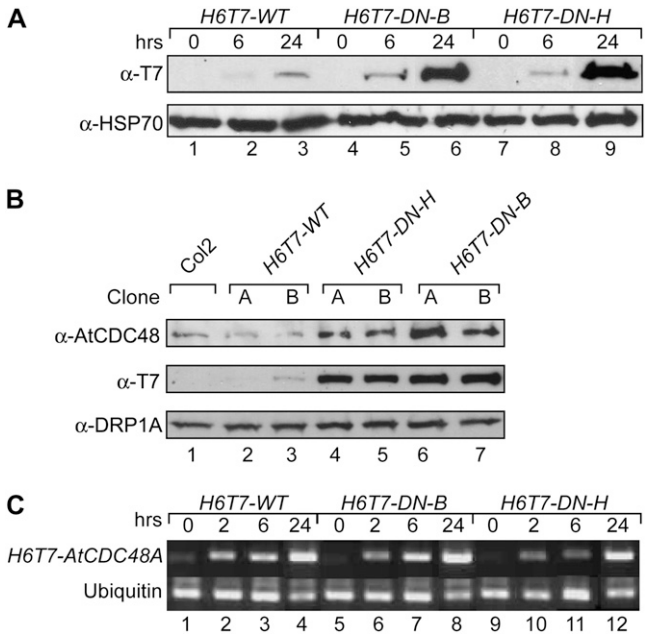

Figure 4. Expression of conditional dominant-negative *Atcdc48A* mutants. A, Time course of transgenic ethanol-induced H6T7-Atcdc48 mutant protein expression. Expression of H6T7-AtCDC48A (H6T7-WT; lanes 1–3), H6T7-Atcdc48^{DN-B} (H6T7-DN-B; lanes 4–6), and H6T7-Atcdc48^{DN-H} (H6T7-DN-H; lanes 7–9) proteins was monitored by SDS-PAGE and immunoblot analysis using an anti-T7 antibody (top) and an anti-HSP70 antibody as a protein load control (bottom). Seedling samples were prepared prior to ethanol treatment (lanes 1, 4, and 7) or after 6 h (lanes 2, 5, and 8) or 24 h (lanes 3, 6, and 9) post-ethanol treatment. B, Immunoblot analysis of endogenous AtCDC48 and H6T7-AtCDC48A protein expression levels from untransformed (Col2, lane 1) and independent transgenic ethanol-induced wild-type H6T7-AtCDC48A (H6T7-WT; lanes 2 and 3), H6T7-Atcdc48A^{DN-H} (H6T7-DN-H; lanes 4 and 5), and H6T7-Atcdc48A^{DN-B} (H6T7-DN-B; lanes 6 and 7). Segments correspond to probing of samples with anti-AtCDC48A (top), anti-T7 (middle), and anti-DRP1A (bottom, load control). Samples were processed and analyzed at 48 h postinduction. C, Reverse transcription-PCR analysis of *H6T7-AtCDC48A* and *H6T7-Atcdc48A^{DN}* gene expression. cDNA was synthesized from total RNA from H6T7-AtCDC48A (H6T7-WT; lanes 1–4), H6T7-Atcdc48^{DN-B} (H6T7-DN-B; lanes 5–8), and H6T7-Atcdc48^{DN-H} (H6T7-DN-H; lanes 9–12) isolated prior to ethanol treatment (lanes 1, 5, and 9) or after 2 h (lanes 2, 6, and 10), 6 h (lanes 3, 7, and 11), or 24 h (lanes 4, 8, and 12) post-ethanol treatment. cDNA fragments were PCR amplified using primers specific to the transgene (top) or the ubiquitin control (bottom).

H6T7-DN-B were analyzed from the root tip to the differentiation zone (Fig. 6). Root cell file organization and differentiation differ according to their longitudinal position (Supplemental Fig. S6). Root cell division occurs predominantly within the zone proximal to the root tip (approximately 100 μm). Within the expansion zone, approximately 300 μm from the root tip, the root cap cells can be seen in the outermost cell layer, and cells start to expand longitudinally. Distal to the region of cell expansion (approximately 1 mm relative to the root tip), root hairs start to emerge from root epidermal cells (trichoblasts) positioned over the junction of two underlying cortex cells (Dolan et al., 1993; Schiefelbein et al., 1997).

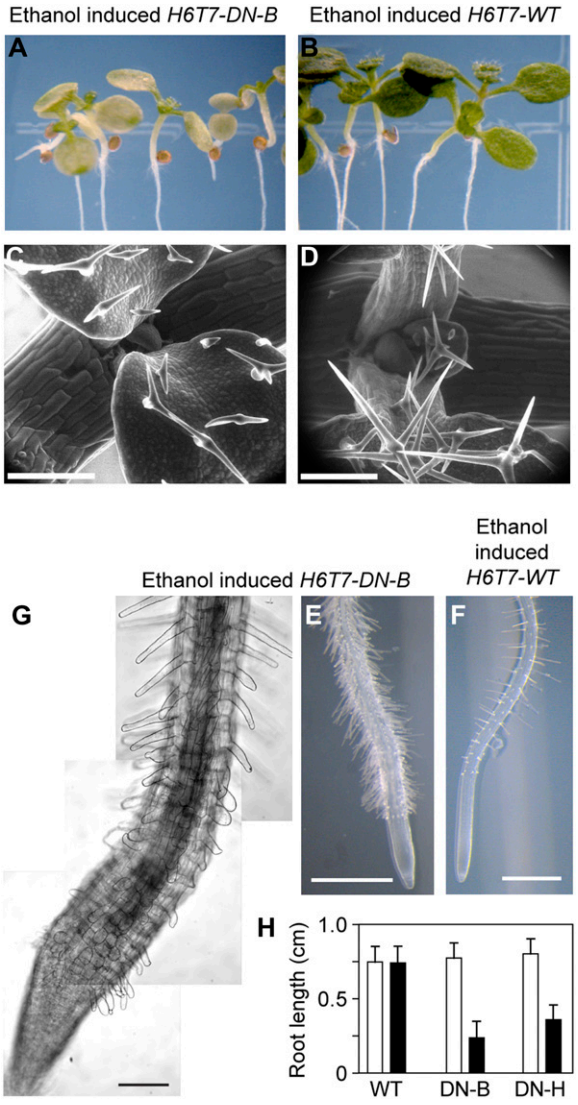

Figure 5. Phenotypic analysis of conditional *Atcdc48A*^{DN} mutant plants. Five-day-old *H6T7-Atcdc48A*$^{DN\text{-}B}$ (*H6T7-DN-B*; A, C, E, and G) and *H6T7-AtCDC48A* (*H6T7-WT*; B, D, and F) seedlings were treated with 2% (v/v) ethanol and imaged after 4 d. A and B, Stereo micrographs of the aerial portion of ethanol-treated *H6T7-DN-B* (A) and *H6T7-WT* (B) plants. C and D, SEM of primary leaves and trichomes from ethanol-treated *H6T7-DN-B* (C) and *H6T7-WT* (D) plants. Scale bar = 200 μm. E and F, Stereo micrographs of roots from ethanol-treated *H6T7-DN-B* (E) and *H6T7-WT* (F) plants. Scale bar = 0.5 mm. G, Higher magnification DIC image composite of an ethanol-treated *H6T7-DN-B* seedling root. Scale bar = 50 μm. H, Total seedling root growth for *H6T7-WT* (WT) and *H6T7-Atcdc48A*^{DN} mutants (ATP binding: DN-B, and ATP hydrolysis: DN-H) was measured after 4 d post-ethanol (black bars) or mock (white bars) treatment. The data represent a minimum sample size of 25 plants for each construct. The SD is represented as error bars for each group.

Prior to the addition of ethanol, *H6T7-DN-B* serial transverse root section analysis indicated no variation in the number of cell files or layers throughout the root length when compared to ethanol-induced *H6T7-WT* wild-type roots (Fig. 6, columns 1 and 2; Dolan et al., 1993). Root hairs were observed to emerge from a root trichoblast cell, as presented previously (Supplemental Fig. S6), in both ethanol-induced *H6T7-WT* and uninduced *H6T7-DN-B* mutant roots (Fig. 6, M and N). In contrast, root hairs of the ethanol-treated *H6T7-DN-B* mutant seedlings were observed immediately above the root cap and emerged from epidermal cells positioned relative to either one or two underlying cortex cells (Figs. 5G and 6F, black arrowhead), thus suggesting cell fate determination defects in the presence of *H6T7-DN-B*. In addition to root hair abnormalities, cell division defects were observed in endodermal and cortex cells (Fig. 6, C, I, L, and O) of ethanol-treated *H6T7-DN-B* plants. The observed cell division defects manifest as either (1) apparent cytokinesis defect, including cell wall stubs (incomplete divisional cell walls), resulting in inappropriate cellular continuity between neighboring endodermal and/or cortical cell files (Fig. 6, L and O, black arrows), or (2) inappropriate cell divisions, including spurious periclinal divisions in the cortex (Fig. 6C, white arrows) and extra anticlinal divisions in the epidermis (Fig. 6I, white arrows). These data demonstrate a role for CDC48/p97 in plant cell division, cytokinesis, and cell fate determination.

DISCUSSION

AtCDC48A Has Multiple Roles during Development

The AAA-ATPase CDC48/p97 in non-plant systems has been shown to function in various pathways, including organelle biogenesis and protein degradation (Peters et al., 1992; Acharya et al., 1995; Rabouille et al., 1995). Localization studies and other studies in Arabidopsis implicate a role for AtCDC48A in plant cytokinesis and cell expansion (Feiler et al., 1995; Rancour et al., 2002, 2004).

To determine if CDC48/p97 function is required for plant cell division, three independent Arabidopsis T-DNA insertion alleles of *Atcdc48A* were identified and characterized. All three *Atcdc48A*$^{T\text{-}DNA}$ alleles were recessive and displayed the same phenotypes, including defects in pollen tube germination and expansion, embryo developmental arrest, and seedling lethality (Figs. 1 and 2). The nature of the variable expressivity of the mutant phenotypes remains to be determined.

AtCDC48A is a highly abundant protein in Arabidopsis (Rancour et al., 2004). One possible explanation for the variable expressivity of the T-DNA mutant phenotypes is that sufficient levels of paternal and/or maternal levels of AtCDC48A are present during embryogenesis to grant some homozygous embryos the capacity to proceed to the next major AtCDC48A-dependent developmental stage. Another possible explanation is that expression of *AtCDC48B* or *AtCDC48C* may compensate for the loss of AtCDC48A in early stages of development, as AtCDC48B and AtCDC48C share 91% and 95% amino acid sequence identity, respectively, with full-length AtCDC48A (Rancour et al., 2002). Nevertheless, analysis of homozygous $Atcdc48A^{T\text{-}DNA}$ mutants demonstrated that AtCDC48A is absolutely required for seedling development.

Morphological analysis of $Atcdc48A^{T\text{-}DNA}$ seedlings has implicated AtCDC48A involvement in multiple seedling developmental processes. Root cells in homozygous *Atcdc48A* seedlings were disorganized and morphologically abnormal suggesting roles for AtCDC48A in cell proliferation and expansion (Fig. 1C) and plasma membrane integrity. CDC48 has been shown to be associated with the plasma membrane in soybean (*Glycine max*; Shi et al., 1995), and Arabidopsis SERK1, a plasma membrane-localized Leu-rich repeat receptor-like Ser Thr kinase, interacts with AtCDC48A (Shah et al., 2002; Rienties et al., 2005). These results indicate that AtCDC48A may have a role in plasma membrane biogenesis and signaling.

To circumvent the range of early plant developmental defects observed in the $Atcdc48A^{T\text{-}DNA}$ mutants, we took an alternative approach, utilizing inducible dominant-negative $Atcdc48A^{DN\text{-}B,\ \text{-}H}$ gene expression, to examine the in vivo role of AtCDC48A in plant growth and development. The presence and accumulation of $Atcdc48A^{DN\text{-}B}$ protein correlated with phenotypes observed throughout the plant, including the arrest of leaf growth and expansion as well as early leaf senescence, alterations in the frequency and distribution of root hairs, and arrest of root growth with defects in cytokinesis and cell expansion (Figs. 5 and 6). The presence of ectopic root hairs in plants expressing $Atcdc48A^{DN\text{-}B}$ suggests that the chaperone may modulate signal transduction pathways and/or transcription factor levels essential for trichoblast/atrichoblast cell fate determination. More importantly, these in vivo dominant-negative mutant studies provided direct evidence that AtCDC48A is required for plant cytokinesis. Consistent with stereotypical plant cytokinesis defects (Lauber et al., 1997; Waizenegger et al., 2000; Strompen et al., 2002; Falbel et al., 2003; Kang et al., 2003), incomplete cell walls and cell wall stubs were observed in induced transgenic $Atcdc48A^{DN\text{-}B}$ root endodermal and cortical cells (Fig. 6, L and O). An intriguing feature of these cytokinesis defects is their prevalence in the endodermal and cortical cell layers and along their interface. The endodermis and cortex arise from a specific longitudinal division of a progenitor cell to give rise to two distinct cell type fates (Dolan et al., 1993). Based on our data, AtCDC48A may have a role in the completion of that longitudinal cell division. Future work is needed to determine the cell fate identity of the resulting cell types after ethanol treatment in the ethanol-inducible dominant-negative mutant plants.

YFP-AtCDC48A Localization

The presence of YFP-AtCDC48A signal in regions of cell proliferation and expansion are consistent with our hypothesis that AtCDC48A plays a role in cell di-

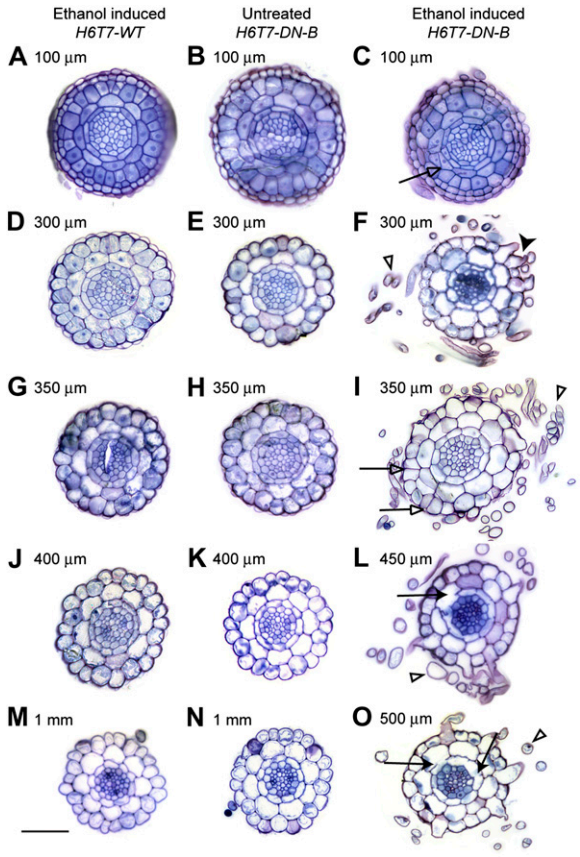

Figure 6. Cell division and trichoblast differentiation are affected in conditional $Atcdc48A^{DN\text{-}B}$ mutant H6T7-AtCDC48A (H6T7-WT; column 1) and H6T7-$Atcdc48A^{DN\text{-}B}$ (H6T7-DN-B; columns 2 and 3) seedlings were analyzed 4 d after 2% (v/v) ethanol (columns 1 and 3) or mock treatment (column 2). Sections were stained with toluidine blue O and imaged by bright-field microscopy. Figure rows correspond to similar distances of tissue sections from the root tip. A root guide is available in Supplemental Figure S6. A to C, Approximately 100 μm above the root tip. D to F, Approximately 300 μm above the root tip corresponding to the division zone. G to I, Approximately 350 μm above the root tip corresponding to the division-expansion transition zone. J to L, Approximately 400 to 450 μm above the root tip corresponding to the expansion zone. M to O, Approximately 500 to 1,000 μm from the root tip corresponding to the expansion-differentiation transition zone. Black arrows highlight apparent cytokinesis defects. White arrows highlight aberrant cell divisions. Black arrowheads indicate root hairs emerging from inappropriate epidermal cells. White arrowheads highlight root hair projections. Scale bars = 50 μm.

vision and expansion. In yeast and *Xenopus*, Cdc48p/p97 have been shown to be associated and to regulate mitotic spindle dynamics (Fröhlich et al., 1991; Cao et al., 2003; Cao and Zheng, 2004; Cheeseman and Desai, 2004). The mitotic spindle localization of AtCDC48A (Feiler et al., 1995) and YFP-AtCDC48A (this study) in plant cells provides additional support that the chaperone may function in plant mitosis.

Following mitosis, AtCDC48A is relocated to the phragmoplast mid-zone and during late telophase, with the reforming nuclear envelope. Our current hypothesis is that AtCDC48A is required for secretory and nuclear membrane dynamics to complete cell division. Consistent with this, CDC48/p97 have been shown to be required for secretory and nuclear membrane fusion and assembly in yeast and mammalian cells (Moir et al., 1982; Fröhlich et al., 1991; Hetzer et al., 2001; Sang and Ready, 2002).

In interphase cells, we observed that YFP-AtCDC48A was predominantly associated with the nucleus and, to a lesser extent, cytoplasm. The various specific patterns of nuclear-associated YFP-AtCDC48A localization observed within plant cell roots have not been reported in any other system. YFP-AtCDC48A was observed in discrete foci within the nucleoplasm and within the nucleolar cavity. The nucleoplasmic structures resemble nuclear bodies, such as speckles, which could implicate a function for AtCDC48A in mRNA processing and export (Pendle et al., 2005). The nucleolar cavity has been suggested to be the site of cleavage and modification of pre-ribosomal RNAs (Beven et al., 1995, 1996; Shaw and Brown, 2004). However, no detectable changes in 18S and 25S RNA processing were observed in *Atcdc48A* mutants line, indicating that the localization of AtCDC48A within the nucleolar cavity is likely unrelated to ribosomal RNA processing. The function of the AtCDC48A containing subnuclear structures remains to be determined.

AtCDC48A Protein Abundance Levels Are Self-Modulated

In addition to its roles in plant growth and development, dominant-negative expression of Atcdc48A$^{DN\text{-}B,\ -H}$ suggested that AtCDC48A may regulate its own steady-state protein level (Fig. 4). Our previous work demonstrates mutant Atcdc48A$^{DN\text{-}B,\ -H}$ protomers are incorporated into hexamers and are essentially ATPase inactive (Park et al., 2007). We found that the UBX-containing protein PUX1 functions to regulate the hexameric structure and ATPase activity of AtCDC48A (Rancour et al., 2004). However, PUX1 was unable to disassemble nucleotide binding or hydrolysis mutants of AtCDC48A complexes (Park et al., 2007). One model to explain the altered Atcdc48A mutant protein accumulation in planta is the inhibition of ATPase-defective hexamers to be disassembled (Park et al., 2007), a likely prerequisite for degradation. Yeast Cdc48p is polyubiquitylated (Mayor et al., 2005), suggesting that disassembly of the CDC48/p97 hexamer into individual subunits is a step in the pathway to its proteasome-dependent degradation. Taken together, these data support a model whereby a certain level or range of AtCDC48A activity is required for cell function and that AtCDC48A protein activity levels are self-maintained to maintain this homeostasis. Future experiments into how the active pool of AtCDC48A activity is sensed and subsequently balanced remain to be studied.

ATP Binding Is More Important Than ATP Hydrolysis for AtCDC48A Function

One subtle but reaffirmed observation was that plants expressing inducible Atcdc48A$^{DN\text{-}B}$ had a more severe phenotype than Atcdc48A$^{DN\text{-}H}$ during seedling growth and development. Given that expression levels of the mutant protein forms were comparable, this would suggest that there are functions for nucleotide substrate-bound form of the enzyme that are distinct from those requiring hydrolysis of that nucleotide substrate. A significant conformational change, including rearrangement of the N-terminal domains, occurs upon nucleotide binding to the CDC48/p97 hexamer (Rouiller et al., 2000). It has been hypothesized that the critical conformational change in the mammalian homolog of AtCDC48A, p97, is a large rearrangement upon nucleotide binding

Table I. *Oligonucleotides used in the study*

Name	Sequence (5′–3′)	Cloning/Screening
SB371	tcagtatcagcggccgcAGTAATCCAAAAGTAGAG	3′ H6T7-AtCDC48A cloning; *Not*I
SB372	CAAACCAGCGTGGACCGCTTGCTGCAACT	Salk T-DNA left border
SB400	ATTTGGGAGAAGTAGTTGG	5′ *AtCDC48A* T-DNA insertion screening
SB401	GTAGAACCACATAAGAATCC	5′ *AtCDC48A* T-DNA insertion screening
SB439	ggaattccatatgCATCATCATCATCATCAC	5′ H6T7-AtCDC48A cloning; *Nde*I
SB504	agagtcgacCATGGAGATTCCGAAGGTTGAAG	5′ AtCDC48A promoter; *Sal*I
SB513	TGGATTCTTATGTGGTTCTAC	5′ *AtCDC48A* T-DNA insertion screening
SB514	CATTCAATAAAATTACACTCA	3′ *AtCDC48A* T-DNA insertion screening
SB656	catatgGATTGAGTTTGAGATTAACGAAAGAG	3′ AtCDC48A promoter; *Nde*I
SB723	gcggccgcCCATGGAGTCAAAGATTCAAATAG	5′ Ethanol-inducible cassette cloning; *Not*I
SB737	gcggccgcTCCTTAGCTCCTGAAAATCTCGAC	3′ Ethanol-inducible cassette cloning; *Not*I

rather than the smaller changes associated with nucleotide hydrolysis. The location and number of molecules of the adaptor protein p47 molecules bound to p97 varies significantly in the nucleotide-free and ADP-bound states, suggesting that p47 requires ATP to form a tight complex with p97 (Dalal and Hanson, 2001). High affinity binding of substrates in the ATP-bound state has been proposed to be a common feature of AAA proteins (Vale, 2000). Our in vivo data is consistent with this proposal.

We conclude that AtCDC48A is required for many cellular processes necessary for plant growth and development. Our data provide new evidence for AtCDC48A function in plant cytokinesis and cell expansion and the ability of the enzyme to self-modulate its steady-state protein levels.

MATERIALS AND METHODS

Oligonucleotides Used in This Study

Oligonucleotide sequences shown in Table I were synthesized by Integrated DNA Technologies. Capitalized sequences represent those complementary to the *AtCDC48A* locus. Underlined lowercase letters in the oligonucleotide sequences indicate added restriction enzyme sites used for cloning.

Isolation of *Atcdc48A* T-DNA Insertion Mutants

Three independent *Atcdc48A* mutant lines containing T-DNA insertions (*Atcdc48A*$^{T\text{-}DNA}$), SALK_064573, SALK_064893, and SALK_116074 (Alonso et al., 2003), were identified using T-DNA Express search algorithms from the Salk Institute Genomic Analysis Laboratory (SIGnAL, http://signal.salk.edu/cgi-bin/tdnaexpress), and seeds were obtained from the Arabidopsis Biological Resource Center (The Ohio State University, Columbus, OH). *Atcdc48A*$^{T\text{-}DNA}$ insertion lines were grown on solidified (0.6% phytoagar) Murashige and Skoog (Murashige and Skoog, 1962) medium (from either Gibco BRL or Caisson Laboratories) and transplanted into soil (either Superfine Germination Mix, Con-rad Fafard; or Metro Mix-360, Sun Gro Horticulture) treated with Adept (Uniroyal Chemical Company) and grown under fluorescent light illumination cycles of 16 h light and 8 h dark at 22°C. The mutant lines were screened for *Atcdc48A*$^{T\text{-}DNA}$ using oligonucleotide primers SB372, SB400, SB401, SB513, and SB514 (Table I). DNA sequencing of the PCR-amplified products determined the T-DNA insertion positions within *AtCDC48A*. The genotype of segregating plants was confirmed by PCR using allele-specific primer pairs. For analysis of *AtCDC48A*$^{T\text{-}DNA}$ mutant developing embryos, siliques were cleared in Hoyers solution (0.25 g [v/w] gum arabic, 3.3 g [v/w] chloral hydrate, 0.15 g [v/v] glycerol in deionized water; Meinke, 1994; Liu and Meinke, 1998) and observed with the bright-field light microscopy. To visualize cell organization in seedling roots, tissue was stained with 0.1 mg/mL propidium iodide for 30 s, washed four times with deionized water, and observed using laser scanning confocal microscopy (LSCM; Nikon Eclipse TE 2000-U, Japan). Captured images were processed using Image J 1.32 (Wayne Rasband, National Institutes of Health) and Adobe Photoshop and Illustrator (Adobe Systems) imaging software on Macintosh computers (Apple Computer).

In Vitro Pollen Germination

Pollen viability and germination was monitored as described (Li et al., 1999). Heterozygote *Atcdc48A;qrt* flowers were harvested and allowed to dehydrate at room temperature for 90 min at 22°C. Pollen grains were transferred to pollen germination media [18% (w/v) Suc, 0.6% (w/v) phytagar, 0.01% (w/v) boric acid, 1 mM $MgSO_4$, 2.5 mM $CaCl_2$, 2.5 mM $Ca(NO_2)_2$, pH 7.0] by tapping mature anthers on the surface of the pollen germination medium. Pollen grains were germinated at 28°C for 6 to 24 h and imaged with a Zeiss Axioskop (Carl Zeiss) equipped with DIC filter sets and a cooled charged-coupled device digital camera containing a 1,317- × 1,035-pixel array (Micromax, Princeton Instruments). Pollen grains were examined also by epifluorescence microscopy after staining with DAPI (100 mM sodium phosphate, pH 7.0, 1 mM EDTA, 0.1% [v/v] TX-100, 0.4 μg mL^{-1} DAPI) in both the epifluorescence (355-nm emission and 420-nm excitation filter set) and the DIC optics modes. Images were captured using IPLab Spectrum (Signal Analytics) and processed using Image J 1.32 and Adobe Photoshop/Illustrator imaging software.

Plant Transformation Vector Construction

A H6T7 epitope tag was generated as described (Rancour et al., 2004). The cDNA encoding H6T7-tagged *AtCDC48A* in pPZP211 was PCR amplified using primers SB439 and SB371, TA-cloned into pGEMT-easy (Promega), and verified by DNA sequence analysis. The *AtCDC48A* native promoter (754 bp upstream of the *AtCDC48A* start codon) was amplified by PCR with SB504 and SB656, restriction digested with *Sal*I and *Nde*I, and subcloned into a *Sal*I- and *Nde*I-digested *H6T7-AtCDC48A*-containing pGEMT-easy vector. The *AtCDC48A* promoter sequence was verified by DNA sequence analysis. The entire construct was subcloned as a *Sal*I and *Kpn*I restriction fragment into pPZP211 (Hajdukiewicz et al., 1994). To generate *AtCDC48A* promoter-EYFP-*AtCDC48A* fusion vector, EYFP was amplified with SB695 and SB683 from pCAM-35S-EYFP-C1 (Preuss et al., 2004) to replace the existing H6T7 tag of *AtCDC48* in pGEMT-easy. This cassette was then subcloned into the *Sal*I and *Kpn*I sites of pPZP211. Images of plants expressing YFP-fused AtCDC48 were taken from an LSC microscope (Nikon) equipped with 40× and plan oil immersion 60× and 90× objectives using a 488-nm argon laser and 565 emission filter with 70-nm bandpass. Images were processed using Image J 1.32 (Wayne Rasband, National Institutes of Health) and Adobe Photoshop/Illustrator (Adobe Systems) imaging software on Macintosh computers (Apple Computer).

Generation of Ethanol-Inducible Dominant-Negative Mutants

The ethanol-inducible transcription factor and promoter from the *alc* cassettes of pSRN1 and pACN1 (pSRNACN_bin; Caddick et al., 1998) were amplified with SB723 and SB737. The amplified fragment was subcloned into the Bsp1201 site of the modified pPZP211 (Bsp1201, compatible with *Not*I, was engineered into the *Hin*dIII site of pPZP211; Scott Michaels, Indiana University) 5′ to *H6T7-AtCDC48A*. The double ATP hydrolysis and binding dominant-negative *Atcdc48A* (*Atcdc48A*^{DN}) mutants were generated as described (Park et al., 2007). The constructs were introduced into wild-type plants (Arabidopsis [*Arabidopsis thaliana*] Columbia-2 ecotype) by a floral dip transformation method (Clough and Bent, 1998). Transgenic plants were selected on solidified (0.6% [w/v] phytoagar) Murashige and Skoog (Murashige and Skoog, 1962) medium containing 100 μg/mL kanamycin. Vertically grown T_2 generations of ethanol-inducible wild-type and dominant-negative *Atcdc48A* seedlings (60 seedlings per 100- × 100- × 15-mm plate) were treated with 1 mL of 0.5%, 1%, and 2% ethanol at the bottom of plates 4 d after germination. Ethanol-treated plates were placed horizontally for 20 min and repositioned to vertical at 22°C. Root length was measured at 1, 2, and 4 d after ethanol treatment. Average and SES were calculated for groups of 24 seedlings. Images of seedling primary leaves and roots were obtained with a stereo microscope (Leica MZ6) equipped with a Leica DFC 480 digital camera (Leica Microsystems Imaging Solutions) 2 h, 6 h, 1 d, 2 d, and 4 d after ethanol treatment. Four days post-ethanol treatment, images of the first true leaves were taken using a Quanta 200 Environmental scanning electron microscope (SEM; FEI) under a 3.87-Torr vacuum using a 20-kV electron beam. Roots were observed by bright-field microscopy with a Zeiss Axioskop microscope, and digital micrograph images were captured with a cooled CCD digital camera and processed as above.

Analysis of Inducible *H6T7-Atcdc48A* Protein, YFP-AtCDC48A, and mRNA Expression

Total protein extracts were prepared from ethanol-inducible transgenic seedlings either mock treated or following the specified time post-ethanol treatment and from transgenic lines expressing YFP and YFP-AtCDC48A. Four seedlings were homogenized in 100 μL of 2× SDS-PAGE sample buffer (Laemmli, 1970) and incubated at 65°C for 15 min. The samples were cleared of insoluble debris by centrifugation at 16,000*g* for 5 min at room temperature, and 15 μL of the supernatant was resolved on a 12.5% (w/v) SDS-polyacryl-

amide minigel and analyzed by immunoblotting with anti-AtCDC48A (Rancour et al., 2002), anti-T7 (Novagen), and anti-YFP antibodies (Rockland; see Supplemental Fig. S1). Densitometric analysis of immunoblot film exposures was performed using a flatbed digital scanner and Image J 1.32 software.

Total RNA was isolated from mock-treated or, at specified times post-ethanol treatment, from whole ethanol-inducible, wild-type, and mutant *Atcdc48A*^{DN} seedlings using TRIzol reagent (Invitrogen) according to the manufacturer's instructions. Total RNA (2 μg) was treated with RQ DNAse (Promega) to eliminate genomic DNA. First-strand cDNA was generated using 1 μg of RQ DNAse-treated total RNA as template, oligo(dT), and Moloney murine leukemia virus reverse transcriptase (Promega) in a 20-μL reaction mixture. A 1-μL aliquot of a 20-fold dilution of the cDNA was subsequently PCR amplified (30 cycles) with the oligonucleotide primer pair for *AtCDC48A* (SB439 and SB36) and ubiquitin (SB747 and SB748) as a control.

Cross-Section Analysis of Wild-Type and *Atcdc48*^{DN} Mutant Roots

The ethanol-inducible wild-type and mutant *Atcdc48A*^{DN} seedlings, before and 4 d after 2% ethanol treatment, were vacuum infiltrated and fixed overnight at 4°C with 4% (v/v) gluteraldehyde in 50 mM potassium phosphate buffer, pH 7.0. Tissue was subsequently rinsed with 50 mM potassium phosphate, pH 7.0, buffer and dehydrated through a graded ethanol series (30%–100%). Tissue was embedded in LR White (EMS). Transverse sections (5 μm) were cut with a Reichert-Jung Ultracut model E microtome (Vienna) and stained with toluidine blue O as described previously (Kang et al., 2001).

Embryo DNA Isolation

Embryos were isolated from developing seed from siliques of self-fertilized *Atcdc48A*$^{T\text{-}DNA}$/+ plants. DNA from individual embryos was isolated according to the following procedure. Isolated embryos were homogenized in 40 μL 250 mM NaOH followed by heating to 100°C for 30 s. To the sample, 20 μL of buffer (500 mM Tris-HCl, pH 8.0, 0.25% [v/v] NP-40) followed by 40 μL of 250 mM HCl were added, and the sample was mixed and incubated at 100°C for 2 min. Samples were cooled to ambient temperature and centrifuged at ambient temperature for 10 min at 16,000*g*. The supernatant was used directly for PCR analysis using primer sets for the gene (SB513 and SB514) and the T-DNA insertion (SB514 and SB372).

Analysis of Complementation of *Atcdc48*$^{T\text{-}DNA}$ Mutants with Native Promoter::YFP-AtCDC48A cDNA

Complementation constructs were originally transformed into *Atcdc48*$^{T\text{-}DNA}$/+ plants. DNA from T_2 plants initially selected for the YFP-AtCDC48A complementation construct by fluorescence microscopic analysis was tested by PCR with primers specific for the uninterrupted endogenous gene (gene; primers SB513 and SB514) and the original T-DNA insertion into the AtCDC48A locus (T-DNA; primers SB514 and SB372). Those plants that tested initially as homozygous for the *AtCDC48A* locus T-DNA insertion were verified by PCR and the latter data are presented (Supplemental Fig. S2).

Immunoblot Analysis of the Expression of YFP-AtCDC48A in Wild-Type and *Atcdc48A*$^{T\text{-}DNA}$ Mutant Plants

Immunoblot analysis of total protein prepared from 4-d-old seedlings of transgenic lines expressing YFP alone in wild-type (AtCDC48A) plants, YFP-AtCDC48A in complemented *Atcdc48*$^{T\text{-}DNA}$/*Atcdc48*$^{T\text{-}DNA}$;*YFP-AtCDC48A* mutant plants, and untransformed wild-type AtCDC48A plants was performed. The immunoblots were probed using anti-GFP (Rockland Immunochemicals) and anti-AtCDC48 (Rancour et al., 2002) antibodies and detected via horseradish peroxidase-conjugates and chemiluminescence exposure to film.

Supplemental Data

The following materials are available in the online version of this article.

Supplemental Figure S1. PCR genotyping of embryos from pale (P) and green (G) developing seed from self-fertilized *Atcdc48*$^{T\text{-}DNA}$/+ plants.

Supplemental Figure S2. PCR verification of native promoter-driven YFP-AtCDC48A cDNA complementation of *Atcdc48*$^{T\text{-}DNA}$ mutant.

Supplemental Figure S3. Analysis of the expression of YFP-AtCDC48A in wild-type and *Atcdc48A* mutant plants

Supplemental Figure S4. AtCDC48 gene expression.

Supplemental Figure S5. Comparative phenotype of inducible ethanol-treated H6T7-WT, H6T7-DN-H, and H6T7-DN-B seedlings.

Supplemental Figure S6. Schematic of a wild-type Arabidopsis root.

Supplemental Movie S1. Native promoter::YFP-AtCDC48A expression and localization in trichomes, leaves, and the shoot apical meristem of homozygous *Atcdc48A*$^{T\text{-}DNA}$ seedlings.

Supplemental Movie S2. The vegetative nucleus moves toward the growing tip of the pollen tub.

Supplemental Movie S3. YFP-AtCDC48A localizes to the nucleus membrane during karyokinesis.

Supplemental Movie S4. YFP-AtCDC48A localization in the nucleus.

ACKNOWLEDGMENTS

We thank Adam Steinberg and Laura Vanderploeg for graphic arts assistance in preparation of the manuscript figures and movies, and members of our laboratory for discussion. We thank Dr. Sara Peterson for training in embedding and sectioning root tissues. SEM imaging was performed in the UW-Madison Plant Imaging Facility.

Received April 23, 2008; accepted July 14, 2008; published July 25, 2008.

LITERATURE CITED

Acharya U, Jacobs R, Peters JM, Watson N, Farquhar MG, Malhotra V (1995) The formation of Golgi stacks from vesiculated Golgi membranes requires two distinct fusion events. Cell **82:** 895–904

Aker J, Borst JW, Karlova R, de Vries S (2006) The Arabidopsis thaliana AAA protein CDC48A interacts in vivo with the somatic embryogenesis receptor-like kinase 1 receptor at the plasma membrane. J Struct Biol **156:** 62–71

Aker J, Hesselink R, Engel R, Karlova R, Borst JW, Visser AJ, de Vries SC (2007) In vivo hexamerization and characterization of the Arabidopsis AAA ATPase CDC48A complex using forster resonance energy transfer-fluorescence lifetime imaging microscopy and fluorescence correlation spectroscopy. Plant Physiol **145:** 339–350

Alonso JM, Stepanova AN, Leisse TJ, Kim CJ, Chen H, Shinn P, Stevenson DK, Zimmerman J, Barajas P, Cheuk R, et al (2003) Genome-wide insertional mutagenesis of Arabidopsis thaliana. Science **301:** 653–657

Alzayady KJ, Panning MM, Kelley GG, Wojcikiewicz RJ (2005) Involvement of the p97-Ufd1-Npl4 complex in the regulated endoplasmic reticulum-associated degradation of inositol 1,4,5-trisphosphate receptors. J Biol Chem **280:** 34530–34537

Beemster GT, Fiorani F, Inze D (2003) Cell cycle: the key to plant growth control? Trends Plant Sci **8:** 154–158

Beuron F, Dreveny I, Yuan X, Pye VE, McKeown C, Briggs LC, Cliff MJ, Kaneko Y, Wallis R, Isaacson RL, et al (2006) Conformational changes in the AAA ATPase p97-p47 adaptor complex. EMBO J **25:** 1967–1976

Beuron F, Flynn TC, Ma J, Kondo H, Zhang X, Freemont PS (2003) Motions and negative cooperativity between p97 domains revealed by cryo-electron microscopy and quantised elastic deformational model. J Mol Biol **327:** 619–629

Beven AF, Lee R, Razaz M, Leader DJ, Brown JW, Shaw PJ (1996) The organization of ribosomal RNA processing correlates with the distribution of nucleolar snRNAs. J Cell Sci **109:** 1241–1251

Beven AF, Simpson GG, Brown JW, Shaw PJ (1995) The organization of spliceosomal components in the nuclei of higher plants. J Cell Sci **108:** 509–518

Beyer A (1997) Sequence analysis of the AAA protein family. Protein Sci **6:** 2043–2058

Caddick MX, Greenland AJ, Jepson I, Krause KP, Qu N, Riddell KV, Salter MG, Schuch W, Sonnewald U, Tomsett AB (1998) An ethanol inducible gene switch for plants used to manipulate carbon metabolism. Nat Biotechnol **16:** 177–180

Cao K, Nakajima R, Meyer HH, Zheng Y (2003) The AAA-ATPase Cdc48/p97 regulates spindle disassembly at the end of mitosis. Cell **115:** 355–367

Cao K, Zheng Y (2004) The Cdc48/p97-Ufd1-Npl4 complex: its potential role in coordinating cellular morphogenesis during the M-G1 transition. Cell Cycle **3:** 422–424

Cheeseman IM, Desai A (2004) Cell division: AAAtacking the mitotic spindle. Curr Biol **14:** R70–72

Clough SJ, Bent AF (1998) Floral dip: a simplified method for Agrobacterium-mediated transformation of Arabidopsis thaliana. Plant J **16:** 735–743

Dalal S, Hanson PI (2001) Membrane traffic: What drives the AAA motor? Cell **104:** 5–8

Dalal S, Rosser MF, Cyr DM, Hanson PI (2004) Distinct roles for the AAA ATPases NSF and p97 in the secretory pathway. Mol Biol Cell **15:** 637–648

Davies JM, Tsuruta H, May AP, Weis WI (2005) Conformational changes of p97 during nucleotide hydrolysis determined by small-angle X-Ray scattering. Structure **13:** 183–195

DeLaBarre B, Brunger AT (2003) Complete structure of p97/valosin-containing protein reveals communication between nucleotide domains. Nat Struct Biol **10:** 856–863

DeLaBarre B, Brunger AT (2005) Nucleotide dependent motion and mechanism of action of p97/VCP. J Mol Biol **347:** 437–452

Dolan L, Janmaat K, Willemsen V, Linstead P, Poethig S, Roberts K, Scheres B (1993) Cellular organisation of the Arabidopsis thaliana root. Development **119:** 71–84

Dreveny I, Pye VE, Beuron F, Briggs LC, Isaacson RL, Matthews SJ, McKeown C, Yuan X, Zhang X, Freemont PS (2004) p97 and close encounters of every kind: a brief review. Biochem Soc Trans **32:** 715–720

Egerton M, Samelson LE (1994) Biochemical characterization of valosin-containing protein, a protein tyrosine kinase substrate in hematopoietic cells. J Biol Chem **269:** 11435–11441

Falbel TG, Koch LM, Nadeau JA, Sack FD, Bednarek SY (2003) SCD1 is required for stomatal cell cytokinesis and polarized cell expansion in Arabidopsis. Development **130:** 4011–4024

Feiler HS, Desprez T, Santoni V, Kronenberger J, Caboche M, Traas J (1995) The higher plant Arabidopsis thaliana encodes a functional CDC48 homologue which is highly expressed in dividing and expanding cells. EMBO J **14:** 5626–5637

Fleming AJ (2006) The co-ordination of cell division, differentiation and morphogenesis in the shoot apical meristem: a perspective. J Exp Bot **57:** 25–32

Fröhlich KU, Fries HW, Rudiger M, Erdmann R, Botstein D, Mecke D (1991) Yeast cell cycle protein CDC48p shows full-length homology to the mammalian protein VCP and is a member of a protein family involved in secretion, peroxisome formation, and gene expression. J Cell Biol **114:** 443–453

Hajdukiewicz P, Svab Z, Maliga P (1994) The small, versatile *pPZP* family of *Agrobacterium* binary vectors for plant transformation. Plant Mol Biol **25:** 989–994

Heim R, Tsien RY (1996) Engineering green fluorescent protein for improved brightness, longer wavelengths and fluorescence resonance energy transfer. Curr Biol **6:** 178–182

Hetzer M, Meyer HH, Walther TC, Bilbao-Cortes D, Warren G, Mattaj IW (2001) Distinct AAA-ATPase p97 complexes function in discrete steps of nuclear assembly. Nat Cell Biol **3:** 1086–1091

Huyton T, Pye VE, Briggs LC, Flynn TC, Beuron F, Kondo H, Ma J, Zhang X, Freemont PS (2003) The crystal structure of murine p97/VCP at 3.6A. J Struct Biol **144:** 337–348

Ikai N, Yanagida M (2006) Cdc48 is required for the stability of Cut1/separase in mitotic anaphase. J Struct Biol **156:** 50–61

Jentsch S, Rumpf S (2007) Cdc48 (p97): a ''molecular gearbox'' in the ubiquitin pathway? Trends Biochem Sci **32:** 6–11

Kang BH, Busse JS, Bednarek SY (2003) Members of the *Arabidopsis* dynamin-like gene family, ADL1, are essential for plant cytokinesis and polarized cell growth. Plant Cell **15:** 899–913

Kang BH, Busse JS, Dickey C, Rancour DM, Bednarek SY (2001) The Arabidopsis cell plate-associated dynamin-like protein, ADL1a, is required for multiple stages of plant growth and development. Plant Physiol **126:** 47–68

Kondo H, Rabouille C, Newman R, Levine TP, Pappin D, Freemont P, Warren G (1997) p47 is a cofactor for p97-mediated membrane fusion. Nature **388:** 75–78

Laemmli UK (1970) Cleavage of structural proteins during the assembly of the head of bacteriophage T4. Nature **227:** 680–685

Lamb JR, Fu V, Wirtz E, Bangs JD (2001) Functional analysis of the trypanosomal AAA protein TbVCP with trans-dominant ATP hydrolysis mutants. J Biol Chem **276:** 21512–21520

Lauber MH, Waizenegger I, Steinmann T, Schwarz H, Mayer U, Hwang I, Lukowitz W, Jürgens G (1997) The Arabidopsis KNOLLE protein is a cytokinesis-specific syntaxin. J Cell Biol **139:** 1485–1493

Leon A, McKearin D (1999) Identification of TER94, an AAA ATPase protein, as a Bam-dependent component of the Drosophila fusome. Mol Biol Cell **10:** 3825–3834

Li H, Lin Y, Heath RM, Zhu MX, Yang Z (1999) Control of pollen tube tip growth by a Rop GTPase-dependent pathway that leads to tip-localized calcium influx. Plant Cell **11:** 1731–1742

Liu CM, Meinke DW (1998) The titan mutants of Arabidopsis are disrupted in mitosis and cell cycle control during seed development. Plant J **16:** 21–31

Lupas AN, Martin J (2002) AAA proteins. Curr Opin Struct Biol **12:** 746–753

Mayor T, Lipford JR, Graumann J, Smith GT, Deshaies RJ (2005) Analysis of polyubiquitin conjugates reveals that the Rpn10 substrate receptor contributes to the turnover of multiple proteasome targets. Mol Cell Proteomics **4:** 741–751

Meijer M, Murray JA (2001) Cell cycle controls and the development of plant form. Curr Opin Plant Biol **4:** 44–49

Meinke DW (1994) Seed Development in Arabidopsis thaliana. Cold Spring Harbor Laboratory Press, Cold Spring Harbor, NY

Meyer HH (2005) Golgi reassembly after mitosis: the AAA family meets the ubiquitin family. Biochim Biophys Acta **1744:** 108–119

Moir D, Stewart SE, Osmond BC, Botstein D (1982) Cold-sensitive cell-division-cycle mutants of yeast: isolation, properties, and pseudoreversion studies. Genetics **100:** 547–563

Muller JM, Deinhardt K, Rosewell I, Warren G, Shima DT (2007) Targeted deletion of p97 (VCP/CDC48) in mouse results in early embryonic lethality. Biochem Biophys Res Commun **354:** 459–465

Murashige T, Skoog F (1962) A revised medium for rapid growth and bioassays with tobacco tissue cultures. Physiol Plant **15:** 473–497

Neuwald AF, Aravind L, Spouge JL, Koonin EV (1999) AAA+: a class of chaperone-like ATPases associated with the assembly, operation, and disassembly of protein complexes. Genome Res **9:** 27–43

Park S, Rancour DM, Bednarek SY (2007) Protein domain-domain interactions and requirements for the negative regulation of Arabidopsis CDC48/p97 by the plant ubiquitin regulatory X (UBX) domain-containing protein, PUX1. J Biol Chem **282:** 5217–5224

Pendle AF, Clark GP, Boon R, Lewandowska D, Lam YW, Andersen J, Mann M, Lamond AI, Brown JW, Shaw PJ (2005) Proteomic analysis of the Arabidopsis nucleolus suggests novel nucleolar functions. Mol Biol Cell **16:** 260–269

Peters JM, Harris JR, Lustig A, Muller S, Engel A, Volker S, Franke WW (1992) Ubiquitous soluble Mg(2+)-ATPase complex. A structural study. J Mol Biol **223:** 557–571

Peters JM, Walsh MJ, Franke WW (1990) An abundant and ubiquitous homo-oligomeric ring-shaped ATPase particle related to the putative vesicle fusion proteins Sec18p and NSF. EMBO J **9:** 1757–1767

Preuss D, Rhee SY, Davis RW (1994) Tetrad analysis possible in Arabidopsis with mutation of the QUARTET (QRT) genes. Science **264:** 1458–1460

Preuss ML, Serna J, Falbel TG, Bednarek SY, Nielsen E (2004) The *Arabidopsis* Rab GTPase RabA4b localizes to the tips of growing root hair cells. Plant Cell **16:** 1589–1603

Rabouille C, Levine TP, Peters JM, Warren G (1995) An NSF-like ATPase, p97, and NSF mediate cisternal regrowth from mitotic Golgi fragments. Cell **82:** 905–914

Rancour DM, Dickey CE, Park S, Bednarek SY (2002) Characterization of AtCDC48. Evidence for multiple membrane fusion mechanisms at the plane of cell division in plants. Plant Physiol **130:** 1241–1253

Rancour DM, Park S, Knight SD, Bednarek SY (2004) Plant UBX domain-containing protein 1, PUX1, regulates the oligomeric structure and activity of Arabidopsis CDC48. J Biol Chem **279:** 54264–54274

Rhee SY, Somerville CR (1998) Tetrad pollen formation in quartet mutants of Arabidopsis thaliana is associated with persistence of pectic polysaccharides of the pollen mother cell wall. Plant J **15:** 79–88

Rienties IM, Vink J, Borst JW, Russinova E, de Vries SC (2005) The Arabidopsis SERK1 protein interacts with the AAA-ATPase AtCDC48, the 14-3-3 protein GF14lambda and the PP2C phosphatase KAPP. Planta **221:** 394–405

Römisch K (2006) Cdc48p is UBX-linked to ER ubiquitin ligases. Trends Biochem Sci **31:** 24–25

Roslan HA, Salter MG, Wood CD, White MR, Croft KP, Robson F, Coupland G, Doonan J, Laufs P, Tomsett AB, et al (2001) Characterization of the ethanol-inducible alc gene-expression system in Arabidopsis thaliana. Plant J **28:** 225–235

Rouiller I, Butel VM, Latterich M, Milligan RA, Wilson-Kubalek EM (2000) A major conformational change in p97 AAA ATPase upon ATP binding. Mol Cell **6:** 1485–1490

Rouiller I, DeLaBarre B, May AP, Weis WI, Brunger AT, Milligan RA, Wilson-Kubalek EM (2002) Conformational changes of the multifunction p97 AAA ATPase during its ATPase cycle. Nat Struct Biol **9:** 950–957

Roy L, Bergeron JJ, Lavoie C, Hendriks R, Gushue J, Fazel A, Pelletier A, Morre DJ, Subramaniam VN, Hong W, et al (2000) Role of p97 and syntaxin 5 in the assembly of transitional endoplasmic reticulum. Mol Biol Cell **11:** 2529–2542

Sang TK, Ready DF (2002) Eyes closed, a Drosophila p47 homolog, is essential for photoreceptor morphogenesis. Development **129:** 143–154

Schiefelbein JW, Masucci JD, Wang H (1997) Building a root: the control of patterning and morphogenesis during root development. Plant Cell **9:** 1089–1098

Schuberth C, Buchberger A (2005) Membrane-bound Ubx2 recruits Cdc48 to ubiquitin ligases and their substrates to ensure efficient ER-associated protein degradation. Nat Cell Biol **7:** 999–1006

Shah K, Russinova E, Gadella TW Jr, Willemse J, De Vries SC (2002) The Arabidopsis kinase-associated protein phosphatase controls internalization of the somatic embryogenesis receptor kinase 1. Genes Dev **16:** 1707–1720

Shaw PJ, Brown JW (2004) Plant nuclear bodies. Curr Opin Plant Biol **7:** 614–620

Shi J, Dixon RA, Gonzales RA, Kjellbom P, Bhattacharyya MK (1995) Identification of cDNA clones encoding valosin-containing protein and other plant plasma membrane-associated proteins by a general immunoscreening strategy. Proc Natl Acad Sci USA **92:** 4457–4461

Strompen G, El Kasmi F, Richter S, Lukowitz W, Assaad FF, Jürgens G, Mayer U (2002) The Arabidopsis HINKEL gene encodes a kinesin-related protein involved in cytokinesis and is expressed in a cell cycle-dependent manner. Curr Biol **12:** 153–158

Vale RD (2000) AAA proteins. Lords of the ring. J Cell Biol **150:** 13–19

Waizenegger I, Lukowitz W, Assaad F, Schwarz H, Jürgens G, Mayer U (2000) The Arabidopsis KNOLLE and KEULE genes interact to promote vesicle fusion during cytokinesis. Curr Biol **10:** 1371–1374

Wang Q, Song C, Yang X, Li CC (2003) D1 ring is stable and nucleotide-independent, whereas D2 ring undergoes major conformational changes during the ATPase cycle of p97-VCP. J Biol Chem **278:** 32784–32793

Woodman PG (2003) p97, a protein coping with multiple identities. J Cell Sci **116:** 4283–4290

Yuan X, Shaw A, Zhang X, Kondo H, Lally J, Freemont PS, Matthews S (2001) Solution structure and interaction surface of the C-terminal domain from p47: a major p97-cofactor involved in SNARE disassembly. J Mol Biol **311:** 255–263

Zhang X, Shaw A, Bates PA, Newman RH, Gowen B, Orlova E, Gorman MA, Kondo H, Dokurno P, Lally J, et al (2000) Structure of the AAA ATPase p97. Mol Cell **6:** 1473–1484

Zimmermann P, Hennig L, Gruissem W (2005) Gene-expression analysis and network discovery using Genevestigator. Trends Plant Sci **10:** 407–409

Zimmermann P, Hirsch-Hoffmann M, Hennig L, Gruissem W (2004) GENEVESTIGATOR. Arabidopsis microarray database and analysis toolbox. Plant Physiol **136:** 2621–2632